IOP Publishing Bioinspir. Biomim. 12 (2017) 016011 doi:10.1088/1748-3190/aa5113

Bioinspiration & Biomimetics

PAPER

RECEIVED
28 July 2016

REVISED
27 October 2016

ACCEPTED FOR PUBLICATION
1 December 2016

PUBLISHED
17 January 2017

Performance variation due to stiffness in a tuna-inspired flexible foil model

Mariel-Luisa N Rosic[1], Patrick J M Thornycroft[1], Kara L Feilich[1], Kelsey N Lucas[1] and George V Lauder[1,2]

[1] The Museum of Comparative Zoology, Harvard University, Cambridge, MA 02138, USA
[2] Author to whom any correspondence should be addressed.

E-mail: glauder@oeb.harvard.edu

Keywords: fish-like swimming, body stiffness, swimming performance

Abstract

Tuna are fast, economical swimmers in part due to their stiff, high aspect ratio caudal fins and streamlined bodies. Previous studies using passive caudal fin models have suggested that while high aspect ratio tail shapes such as a tuna's generally perform well, tail performance cannot be determined from shape alone. In this study, we analyzed the swimming performance of tuna-tail-shaped hydrofoils of a wide range of stiffnesses, heave amplitudes, and frequencies to determine how stiffness and kinematics affect multiple swimming performance parameters for a single foil shape. We then compared the foil models' kinematics with published data from a live swimming tuna to determine how well the hydrofoil models could mimic fish kinematics. Foil kinematics over a wide range of motion programs generally showed a minimum lateral displacement at the narrowest part of the foil, and, immediately anterior to that, a local area of large lateral body displacement. These two kinematic patterns may enhance thrust in foils of intermediate stiffness. Stiffness and kinematics exhibited subtle interacting effects on hydrodynamic efficiency, with no one stiffness maximizing both thrust and efficiency. Foils of intermediate stiffnesses typically had the greatest coefficients of thrust at the highest heave amplitudes and frequencies. The comparison of foil kinematics with tuna kinematics showed that tuna motion is better approximated by a zero angle of attack foil motion program than by programs that do not incorporate pitch. These results indicate that open questions in biomechanics may be well served by foil models, given appropriate choice of model characteristics and control programs. Accurate replication of biological movements will require refinement of motion control programs and physical models, including the creation of models of variable stiffness.

1. Introduction

Variation in caudal fin shape and stiffness is likely a major predictor of swimming performance in fishes (Breder 1926, Affleck 1950, Alexander 1965, McHenry *et al* 1995, Gibb *et al* 1999, Lauder *et al* 2012). The semilunate tails of the scombrid fishes are of particular interest due to their association with high-speed economical swimming (Dewar and Graham 1994, Sepulveda and Dickson 2000, Katz *et al* 2001, Nauen and Lauder 2002). The high aspect ratio shape, stiffened fin rays, and fused caudal vertebrae of tuna tails all contribute to high thrust production at a minimal drag cost (Fierstine and Walters 1968, Long 1992, Westneat *et al* 1993). The semilunate tail is well studied using theoretical and mathematical models (Lighthill 1970, Wu 1971, Chopra and Kambe 1977, Karpouzian *et al* 1990), computational fluid dynamics models (Borazjani and Daghooghi 2013), and some mechanical models (Affleck 1950, Feilich and Lauder 2015). Given the importance of the semilunate tail in economical cruising in fishes, it is prudent to build more sophisticated models to determine which physical factors contribute the most to swimming performance. However, many mechanical modeling studies of flexible flapping propulsion have used very simple models with either rectangular or NACA foil-like geometry (e.g. Dewey *et al* (2013), Kancharala and Philen (2014), Shelton *et al* (2014) and Quinn *et al* (2014a, 2014b)). Among these studies, few have looked at the interaction of shape and stiffness, even though stiffness is considered an important feature of tuna tails (Feilich and Lauder 2015). To complicate matters, to our knowledge there is currently only one study of *in vivo* tuna kinematics available (Donley and Dickson 2000) with sufficiently detailed kinematics to

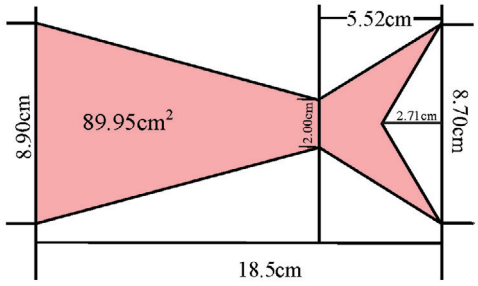

Figure 1. Design and dimensions of tuna-inspired hydrofoils, with a high-aspect ratio tail region. This shape is identical to foil 1 in Feilich and Lauder (2015).

allow for comparisons of model kinematics to live tuna kinematics.

Recent efforts to determine the effect of shape on undulatory propulsion have used passive flexible foils to investigate the effect of stiffness and shape. An earlier analysis of fish tail shape models suggests that while high aspect ratio models may sometimes perform well in comparison to other shapes, tail performance cannot be determined from shape and stiffness alone (Feilich and Lauder 2015). Given a range of stiffnesses, there was no single tail shape that maximized both thrust and economy for all stiffnesses. It was not possible to predict a foil's performance based on its stiffness and shape as these interacted in complex ways in their effects on thrust production, power, and cost of transport (Feilich and Lauder 2015). While that study shed light on the interacting effects of shape and stiffness on swimming performance, it did so using only three different stiffnesses and four different shapes over a narrow range of driving motions, limited to those that produced self-propulsion in each foil type. Self-propulsion (*sensu* Lauder *et al* 2012, Kancharala and Philen 2014, Quinn *et al* 2014b, Feilich and Lauder 2015, Lucas *et al* 2015) here refers to the condition where thrust and drag forces balance, and for a given pattern of motor actuation, occurs at a specific speed called the self-propelled speed. Later work demonstrated that refinements in the kinematic program driving flapping foil models could produce considerably more fish-like kinematics (Lucas *et al* 2015).

In this study, we focused on the performance of one passively flexing tuna-inspired-tail shape (figure 1) manufactured in a wide range of stiffnesses comparable to the range of stiffnesses exhibited along the bodies of fish (McHenry *et al* 1995, Long 1998). Our goals in this study were: (1) to extend previous studies (e.g. Feilich and Lauder (2015)) of simple passive tail models by examining a much wider range of tail stiffnesses and swimming frequencies than previously studied, (2) to collect detailed data on the kinematics, thrust, and efficiency of each foil to see how these variables vary with stiffness, and (3) to compare quantitative kinematic data on foil motion with the only available *in vivo* data on tuna body kinematics from Donley and Dickson (2000), thereby assessing the ability of foil models to replicate biological motions.

Table 1. Physical characteristics and material properties of the foils used in this study with abbreviations and colors for foil identification throughout this paper.

Foil	Mass (g)	Thickness (cm)	Flexural stiffness of the material, EI (N cm^2)	EI standard error
S1	1.30	0.020	0.05	0.003
S2	2.20	0.027	0.16	0.012
S3	5.63	0.063	0.34	0.000
S4	8.55	0.093	0.58	0.006
S5	11.55	0.113	0.69	0.003
S6	14.60	0.139	0.77	0.010

We hypothesized that the stiffest foils would generate the most thrust based on the results of Katz and Weihs (1978) and Shelton *et al* (2014), which show that stiffer foils studied consistently had a higher coefficient of thrust than more flexible foils, although the Katz and Weihs (1978) foils were high aspect ratio compared to those used here. Further, based on Shelton *et al* (2014), we hypothesized that the most flexible foils would generally be the most efficient. Finally, following the results of Lucas *et al* (2015), we hypothesized that a zero-degree angle of attack motion program (described below) that constantly adjusts foil leading edge pitch during swimming would mimic live tuna motion more accurately than programs without any pitch.

2. Materials and methods

2.1. Foil design and flexural stiffness

To model the shape of a tuna tail, our foil design was identical to Shape 1 in Feilich and Lauder (2015) and has a narrow caudal peduncle anterior to a forked, high-aspect ratio tail (figure 1). This shape was laser-cut from six plastics (ARTUS Corp, Englewood, NJ, USA) of a wide range of thicknesses, and hence, stiffnesses (covering the stiffness range naturally occurring in live fishes; see McHenry *et al* (1995) and Long (1998)), with holes cut into the leading edge for attachment to the leading edge flat shaft as in our previous research (Lucas *et al* 2015). The foils were named with reference to their stiffness, with S1 being the least stiff and S6 the most stiff (table 1). Three-point bending tests were conducted in order to obtain values for the flexural stiffness of each material, which are recorded in table 1 along with the naming and color foil identification scheme used throughout this study.

2.2. Experimental setup

Our experimental setup closely follows that of previous flapping foil experiments (Shelton *et al* 2014, Quinn *et al* 2014a, 2014b, Feilich and Lauder 2015, Lucas *et al* 2015). Briefly, each foil was screwed into a flat shaft at the leading edge, with an ATI-Nano17 six-axis force-torque transducer (ATI Industrial Automation, Apex,

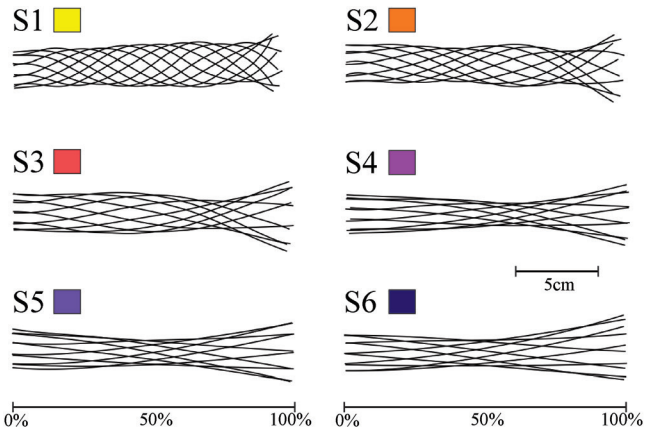

Figure 2. Midline kinematics for each foil stiffness at 2.5 Hz heave frequency and 1.0 cm heave amplitude, with no pitch, at a flow speed of 0.15 m s^{-1}. 0% represents the leading edge of the foil attached to the rod; 100% is the tail tip. The Strouhal number ranged from 0.53 to 0.64 for the foils presented. S1 is the least stiff foil and S6 is the stiffest. Colors correspond to those in table 1 and are used in subsequent figures for ease of foil identification.

NC, USA) fitted to the top of the shaft. This shaft was attached to a carriage placed over the recirculating flume in which the foils swam. The shaft was moved by a computer-controlled mechanical actuator located on the carriage. Custom LabVIEW programs (National Instruments Corp., Austin, TX, USA) were used to control flow speed, foil heave (lateral motion), pitch (rotation of the shaft), and flapping frequency. All trials were conducted at a flow speed of 0.15 m s^{-1}, or 0.8 l s^{-1}. For most trials, the foils were actuated using a heave-only motion program, in which the leading edge shaft was moved laterally in heave with no pitch. Heave amplitudes ranged from 0.2–1.0 cm, in 0.2 cm steps. Leading-edge flapping frequencies ranged from 0.5 to 3.5 Hz, in 0.25 Hz steps. For the 'zero angle of attack' motion program following Lucas *et al* (2015), foils swam at specific heave amplitudes and frequencies while pitch was constantly adjusted during swimming to maintain a zero-degree geometric angle of attack into the oncoming flow. The zero angle of attack motion program was used with the S3 foil as part of the comparison with tuna kinematics.

To account for rotation of the force transducer during zero angle of attack motion, streamwise force or thrust (T) was recovered from measured forces on the transducer's x ($F_{x,\mathrm{meas}}$) and y ($F_{y,\mathrm{meas}}$) axes as follows (Lucas *et al* 2015):

$$T = F_{x,\mathrm{meas}} \cos\theta + F_{y,\mathrm{meas}} \sin\theta, \quad (1)$$

where θ is the pitch. This enabled calculation of non-dimensional thrust coefficient (C_T):

$$C_T = \frac{T}{A_t \rho}, \quad (2)$$

where A_t is the surface area of the foil upon which the forces act and ρ is the fluid density. Foil swimming efficiency, or the Froude efficiency, was calculated as:

$$\mathrm{Eff} = \frac{T \cdot S}{\rho}, \quad (3)$$

where S is the swimming speed and P the power consumed by the apparatus to move the foil (Read *et al* 2003).

2.3. Midline kinematics

High-speed videos of the swimming foils were taken using selected motion programs to match the motions of living tuna (at 3 Hz driving frequency, figure 6), and to highlight kinematics under a driving frequency that represented an inflection point in performance measures (2.5 Hz, figure 2). Videos were taken in ventral view using a 45° mirror positioned below the flow tank with a Photron PCI-1024 high-speed camera (1 megapixel resolution) at 250 frames s^{-1}. Midlines were traced at 0.04 s time intervals over seven cycles of motion in a custom MATLAB program (The MathWorks, Inc., Natick, MA, USA). Midline kinematic data for Kawakawa tuna (*Euthynnus affinis*) swimming in a flow tank were used with permission from Donley and Dickson (2000). The tuna had a 25 cm fork length, and was swimming at 1.35 l s^{-1}, at a Strouhal number of 0.27. Flapping foil models represent only the thrust-generating region of a swimming fish (Shelton *et al* 2014, Lucas *et al* 2015). To facilitate comparison between these models and the tuna kinematics, the corresponding region of the tuna's body needed to be identified. Noting that the leading and trailing edges of the foil were the same height, we approximated the thrust producing region of the tuna body as the region posterior to the longitudinal position of maximum body depth. This longitudinal position corresponds to the point at which caudal fin height and body depth are approximately equal, mimicking the structure of the foil shape. To determine where along the length of the body maximum depth occurs, the length, body depth, and longitudinal position along the length of tuna specimens were measured from one *E. affinis* and eight *Euthynnus alleteratus* specimens from the Harvard University Museum of Comparative Zoology (MCZ 162959; 17294; 17309; 17249a–d; 16848a,b).

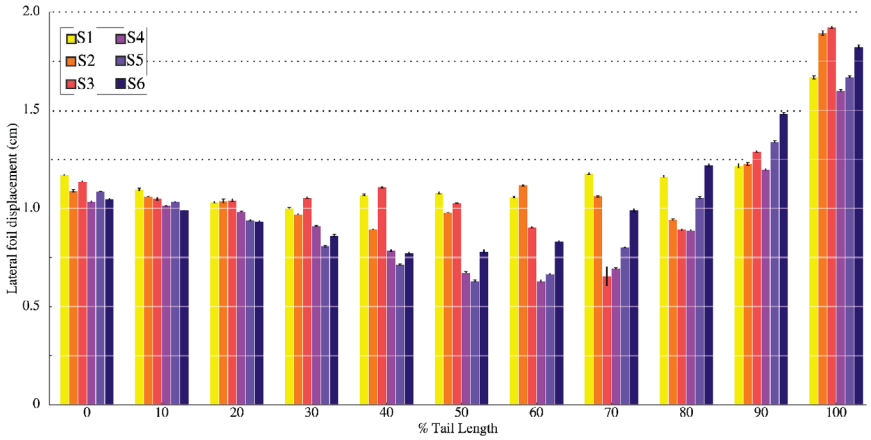

Figure 3. Total lateral displacement of the foil tail tip from the foil midline (0 on the *y*-axis) ± SEM, at a 1 cm heave amplitude and 2.5 Hz heave frequency. 0% on the *x*-axis represents the leading edge of the foil immediately behind the rod attachment. The narrowest part of the foil is at 70% length.

All of these specimens were of lengths similar to the 25 cm fork length tuna used in Donley and Dickson (2000). The average location of maximum body depth on these nine fish was approximately 28–30% of total body length from the snout. Therefore, data were analyzed with the '0% along body length' (leading edge) point on the foils matched to the '30% total body length' point on live tuna in order to best match the lateral amplitude of excursion of the foil with the tuna. Therefore, only displacement data from 30%–100% total body length of the live tuna from the Donley and Dickson (2000) paper were used for comparison with the foil kinematics.

2.4. Statistical analysis

Two-way ANOVA statistical tests were carried out using JMP Pro 11 (SAS Institute Inc., Cary, NC, USA) to identify the effects and interactions of a foil's stiffness and the location along the foil's length on the lateral displacement. Two separate three-way ANOVA analyses were carried out to identify the effects and interactions of a foil's stiffness, heave amplitude, and flapping frequency on the dependent variables of coefficient of thrust, and efficiency. These tests were used to reveal which factors may be contributing to the observed differences across the foils in the various motion programs.

3. Results

3.1. Midline kinematics

Midline kinematics envelopes (figure 2) revealed the presence of minimum lateral displacement located somewhere between 50–80% of the foil's length, at or near the location of the narrowest portion of the foil's 'body', corresponding to the caudal peduncle of a swimming fish. This location with minimum displacement was positioned most posteriorly in the more flexible foils, and moved anteriorly as foil stiffness increased. The greatest decrease in lateral displacement occurred in foils of intermediate stiffnesses, with comparatively small decreases in the stiffest and most flexible foils. In many of the foils, a local increase in lateral displacement occurred immediately anterior to the minimum in lateral displacement (figures 2 and 3), and a general trend of increase in wavelengths along the foil with increasing stiffness was observed.

Quantitative examination of the foils' lateral displacement (figure 3) did not indicate any particular trend in tail-tip displacement magnitude with stiffness or motion program. The intermediate-stiffness foil S3 experienced the greatest tail-tip displacement, followed by the more flexible S2 and the very stiff S6 (figure 3). The foils of intermediate stiffness had more variation in lateral displacement along their lengths. The two-way ANOVAs of these kinematics data show highly significant effects of longitudinal position ($p < 0.0001$), stiffness ($p < 0.0001$), and position * stiffness interaction ($p < 0.0001$) on lateral displacement.

3.2. Foil performance: thrust and efficiency

At all combinations of heave amplitude and flapping frequency, the most flexible foils (S1, S2) generated very little thrust, but the pattern of thrust production was more complicated for the other foils (figure 4). At the highest heave amplitudes and frequencies, the intermediate stiffness foils (S3, S4) generated the most thrust, followed by the stiffest foils (S5, S6) (figure 4). At slightly lower frequencies (1.75–2.25 Hz), however, foil S6 generated the most thrust. Across all stiffnesses, the foils operated in drag at the lowest heave amplitudes and frequencies. Thrust production increased and became positive with both increasing heave amplitude and flapping frequency (figure 4).

Like thrust coefficient, efficiency increased with both heave amplitude and flapping frequency. The most flexible foils were nearly always the most efficient, though efficiency may be in part dictated by foil mass. At the highest heaves and frequencies, the foils' efficiencies could be ranked in order of their mass (table 1),

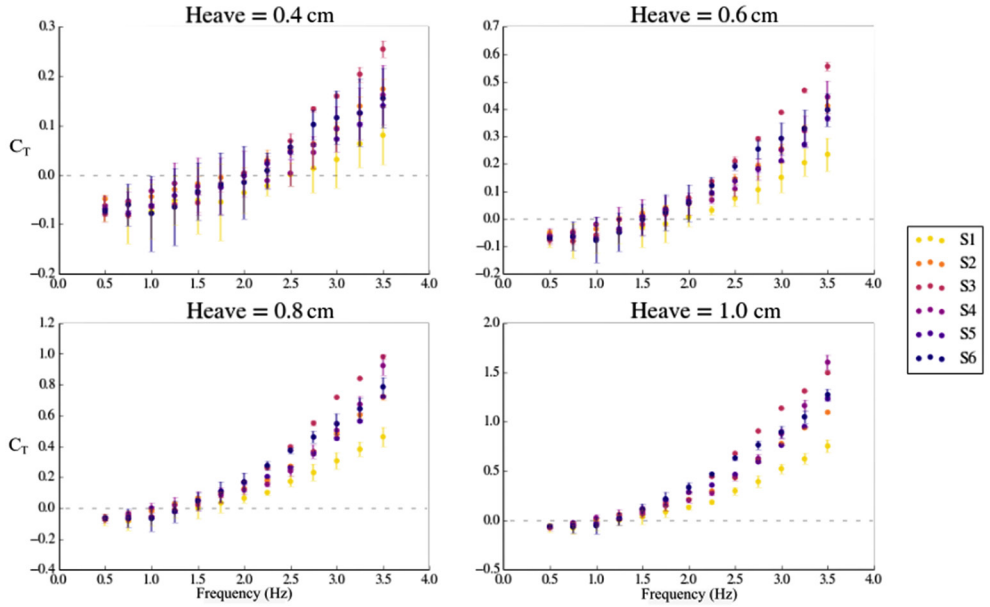

Figure 4. Coefficient of thrust (C_T) for each foil stiffness at four different leading edge heave amplitudes. Thrust increased with heave frequency for all foil stiffnesses, but the effect of stiffness on thrust was non-linear.

with S1 being the most and S6 the least efficient foils (figure 5). This mass dependency did not hold at lower flapping frequencies. For example, foil S2 had much higher efficiency than all other foils when moving at 1.5 Hz in 0.6 cm, 0.8 cm and 1.0 cm heave amplitudes, and S4 had the greatest efficiency at 1.0 Hz and 1.0 cm heave amplitude (figure 5). Generally, however, the efficiency curves for all foils initially increased with flapping frequency before eventually plateauing (figure 5).

A three-way ANOVA indicated that foil stiffness, heave, and frequency and all of their interactions had significant ($p < 0.0001$) effects on the resulting thrust coefficient. Similarly, another three-way ANOVA showed that stiffness ($p < 0.0056$), frequency ($p < 0.0001$), heave ($p < 0.0001$) and the frequency * heave interaction term ($p < 0.0001$) all had significant effects on efficiency, but stiffness * heave, stiffness * frequency, and the stiffness * heave * frequency interaction terms were all non-significant.

3.3. Comparison to live tuna kinematics

Heave-only with 1.0 cm leading edge heave amplitude, zero angle of attack with 1.0 cm leading edge heave amplitude, and zero angle of attack with 0.5 cm leading edge amplitude motion programs all led to very different foil kinematics which resembled live Kawakawa tuna (*E. affinis*) kinematics from Donley and Dickson (2000) to varying degrees (figure 6). In all three cases, the most evident difference between the foils and tuna was the minimum in lateral displacement that the tuna exhibited around 20–40% of its 'thrust producing' body length, (44–58% total length) (figure 6). Taken in the order presented, the three foil motion programs represent a progression toward more tuna-like kinematics.

The heave-only program kinematics matched the kinematic profile of the tuna only over the last third of its length (figure 6). The lateral displacement of the foil using this program was relatively constant along the first two-thirds its length, contrasting with the changing lateral displacement along the length of the tuna (figure 6). Adding zero angle of attack pitching motions initially did little to improve the match to tuna kinematics; in fact, at a 1.0 cm heave amplitude, this led to extreme lateral displacement in the middle of the foil and tail kinematics dissimilar to the tuna (figure 6). When the leading edge heave amplitude was reduced to match the tuna's lateral displacement at the position of the tuna's body corresponding to the foil's leading edge, the most tuna-like kinematics were achieved (figure 6). This program—zero angle of attack with 0.5 cm leading edge heave amplitude—led to a foil kinematic profile that matched the tuna particularly well over the last third of the foil's length (figure 6). Small differences between the tuna and the foil were still evident in places, including the aforementioned minimum in the tuna kinematics at around half of the tuna's body length (figure 6).

4. Discussion

4.1. Effects of stiffness

From these results, it is evident that the effects of stiffness on lateral displacement, efficiency, and thrust are complex and not easily predicted. For example, we would expect that the stiffest foil, S6, would generate the greatest thrust based on studies such as Shelton *et al* (2014). Theoretically, the stiffer foils should be able to exert greater force on the surrounding fluid during undulatory motion. This did not hold for the tuna-inspired foil shape. The S6 foil consistently

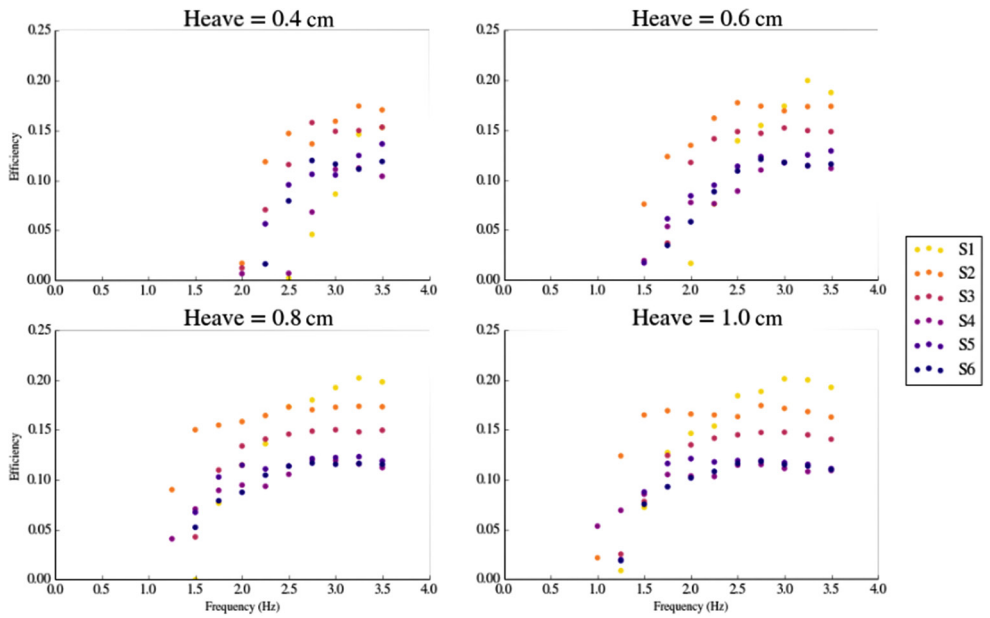

Figure 5. Variation in foil efficiency with frequency at four different leading edge heave amplitudes. Negative efficiencies that occurred at low frequencies are not shown. Efficiency initially increased, then plateaued or even decreased with frequency.

generated the same or less thrust than the other foils, particularly at high frequencies. This suggested that thrust generation must be contingent upon more than the stiffness of a foil. Foils S1 and S2, the most flexible foils, are by far the most efficient foils tested within the set parameter space, with S2 in particular exhibiting clear peaks in efficiency at heave frequencies of 1.0–2.0 Hz. Swimming efficiency also shows a clear mass-dependence (table 1, figure 5) and a reduction in inertial effects may be one reason why the lowest mass foils incur the lowest swimming costs (figure 5). Although the most efficient foils at the higher frequencies were the most flexible, at some point we would expect that there would be a limit where greater flexibility would lead to decreased efficiency. Measuring efficiency with extremely flexible foils that generate little thrust would certainly be a challenge, but determining the limit at which flexural stiffness no longer increases efficiency is an interesting direction for future work.

In a broader perspective, the conclusions drawn from earlier works have not always been in agreement. For instance, in contrast to our findings, Root and Liew (2014) used computational and mathematical modeling to conclude that robotic fish models with the greatest stiffnesses were the best performers with respect to both speed and efficiency. Despite this lack of agreement, a few general trends have emerged in a number of earlier works and are supported by the present study. Intermediate stiffnesses often appear to lead to desirable swimming performance outcomes; experimental results from Kancharala and Philen (2014) showed an increase in stiffness leads to a general decrease in both thrust and efficiency, and that too much flexibility eventually leads to drag production. They proposed that each individual motion program (heave amplitude, frequency, and pitch) has its own optimal foil stiffness (Kancharala and Philen 2014). A number of other works have further developed this idea and demonstrated that multiple desirable parameters, namely, thrust and efficiency, will not necessarily be maximized simultaneously. Shelton *et al* (2014) describe a complex relationship between stiffness and performance, where at low frequencies their stiff foil swam at a higher efficiency than their flexible foil. As frequency increased, a critical flapping frequency was achieved at which these two foils of very different stiffness could swim with similar efficiency, but while producing very different thrust. In fact, the stiffer foil always achieved larger thrust magnitudes than the flexible foil. At high flapping frequencies, then, there was a tradeoff between maximizing thrust and maximizing frequency. Feilich and Lauder (2015) and Lucas *et al* (2015) both reach similar conclusions, and our findings are in line with these recent works.

In sum, the findings of these previous studies are predicted, and most succinctly explained, by Katz and Weihs (1978, p 497): 'Slight flexibility can lead to a moderate gain in efficiency with a loss in thrust that is still tolerable'. Regardless of the foils tested, the relationship between stiffness, thrust and efficiency is complex and case-specific, and all of these previous studies assert the importance of body stiffness in fish swimming.

4.2. Foil kinematics

Predicting foil swimming performance from kinematic patterns has proven challenging. Even simplified fish models such as flexible rectangular foils provide unclear guidance in attempts to predict which foil motions generate the most thrust or are the most efficient (Ahlborn *et al* 1997, Anderson *et al* 1998, Zhu 2007, Shelton *et al* 2014, Lucas *et al* 2015). Particularly, for the tuna tail-inspired foils, S3 and S4 consistently have

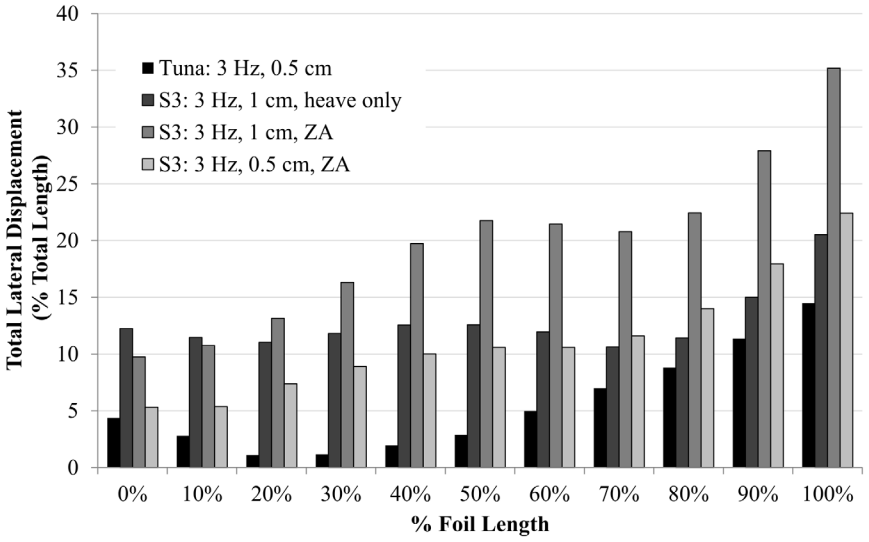

Figure 6. The total lateral displacement as % of length posterior to the point of maximum body depth for the tuna, and % total foil length for the foils, ±SEM along the posterior 70% of a tuna body swimming at 1.35 l s^{-1}, compared to that of selected foil models swimming at 0.8 l s^{-1}. Foil motion programs are reported in the legend as foil: heave frequency, heave amplitude, and either heave only or zero angle of attack (ZA). Along the *x*-axis, 0% represents the 30% total length mark for the tuna (near the position of maximum body depth), and the leading edge of the foil. Displacement is expressed relative to total length of the tuna specimen for the tuna data, and foil length for the foils.

the most 'fish-like' kinematic profiles of all the foils (figure 2), and therefore could be expected to exhibit high performance. Yet, they perform poorly in many circumstances, for instance at 0.4 cm heave and 2.5 Hz frequency, S4 has by far the lowest efficiency and S3 the lowest thrust coefficient.

Across all kinematic profiles, a minimum amplitude in the body waveform occurs at the caudal peduncle directly posterior to a local region of large lateral displacement. The greater the lateral displacement in this region and smaller the minimum lateral displacement, the larger the tail-tip displacement (figures 2 and 3). Lucas *et al* (2015), drawing from earlier works such as Müller *et al* (1997) and Wolfgang *et al* (1999), suggested that large displacements, particularly at the tail tip, help to entrain and accelerate larger volumes of fluid, leading to increased force production when the fluid is later shed as vortices in the wake. Thus, we might expect that, as S3 had the greatest tail-tip displacement, it experienced large thrust—and we do indeed see this. However, the S2 foil, which had a similar kinematic profile, always generated relatively low thrust, indicating that kinematic analyses in isolation do not necessarily predict performance. Tail tip amplitude is a reasonable surrogate for the width of the hydrodynamic wake, and stiffness of the foil material could influence locomotor thrust and efficiency by altering wake width. Wake width, especially when resonant effects are important, could be substantially different from the amplitude of leading edge oscillation.

Further evidence of the limitations of kinematics in predicting performance comes from comparisons of other foils. The most striking example is the comparison of S3 and S4: these two foils generated the most thrust (figure 4), but S3 displayed exaggerated bending along its length whereas S4's profile exhibited less bending, similar to the stiffer S5 and S6 foils (figure 2). In addition, foil S3 had the greatest tail-tip displacement and S4 had the least, even though their stiffnesses are similar (figures 2 and 3). Again, based on the findings from rectangular foils, these kinematic profiles might suggest that S3 would perform well while S4 would not, which is contrary to what we observed. Exceptions to the 'rules' of rectangular foil kinematics and performance relationships suggest other, potentially biologically relevant, kinematic strategies to improve swimming performance. Particularly, it appears that a lateral displacement minimum located at the peduncle in conjunction with a local area of large lateral displacement, as in S3, enhances thrust; nevertheless, higher stiffness bodies may produce comparable thrust with different kinematics (figures 2 and 4).

The complexity of the relationship between kinematic patterns and measured thrust and efficiency of tuna tail-shaped foils may in part be due to patterns of wake recapture. Feilich and Lauder (2015) noted that the tail region of tuna-shaped foils can experience dramatically different flow regimes, depending on the motion program, as flow incident to the tail is greatly altered by motion of the foil 'body' upstream. The tuna tail shape in particular enhances the possibilities of wake recapture and thrust enhancement at the tail due to the narrowing of the body near the caudal peduncle region, and the resulting flow separation that occurs from the sharp trailing edge of the 'body' (Feilich and Lauder 2015). The complexity of the phase relationship between two undulating anatomical structures (of fish) or foil elements, and the dependence of thrust and efficiency on their relative motions, may explain the challenge of predicting

thrust and efficiency from foil kinematics. Throughout the existing literature on fish locomotion, evidence shows that live fish and swimming foils can exploit vortex shedding in order to minimize cost of transport, maximize efficiency, and even potentially enhance thrust (Drucker and Lauder 2001, Akhtar *et al* 2007).

4.3. Comparison to live tuna

By adding zero angle of attack motion and matching the prescribed heave amplitude and frequency of the foil to known tuna kinematics (Donley and Dickson 2000), we were able greatly improve the foil model's representation of the tuna (figure 6). The zero angle of attack motion acts to constantly change the pitch angle of the foil based on the direction of the oncoming flow in a manner that resembles the body motions of a swimming fish. Lucas *et al* (2015) found that applying this zero angle of attack program leads to foil kinematics more representative of swimming kinematics in fishes. We corroborated this finding: introducing the zero angle of attack motion program greatly improved the match between foil and tuna kinematics. This indicates that the replication of fish-like motions by swimming flexible foils with a flat leading edge needs to involve both pitch and heave movement, and that phasing these two motions in a manner comparable to achieving a zero-degree geometric angle of attack generates the most fish-like kinematics. A zero angle of attack motion that minimizes leading edge separation is not necessarily also optimal in foils with a rounded leading edge, such as fish caudal fins or airfoil geometries, if the effective angle of attack is small (Read *et al* 2003, Borazjani and Daghooghi 2013). However, even NACA airfoil shapes, when moved in heave or in heave plus small pitch rotation angles, can incur leading edge separation and potentially increase swimming efficiency with leading edge suction. When viewed in the light of the clear improvements in multiple performance metrics—i.e. thrust, efficiency, self-propelled swimming speed, and cost of transport (Lauder *et al* 2012, Lucas *et al* 2015, Quinn *et al* 2015)—associated with the addition of pitch, and particularly zero angle of attack programs, our findings further highlight the need to emulate the animal's body motions more closely while using physical models of their locomotion.

There are many limitations to the approach of using simple foils models to study a complex system like the tail of tuna. Most significantly, our model was flat, smooth and essentially 2D. While the complex shape of the foil allowed for some variation in flexural stiffness along the length and replicated the high aspect ratio tail of a tuna with the relatively narrow peduncle, each model was nevertheless constructed from a plastic of uniform material stiffness. In addition, our foils were passive and controlled at the leading edge, whereas live tuna actively control musculature along the length of the body (Ellerby *et al* 2001). Together, these differences could explain why the foil models showed greater lateral displacement anteriorly compared to live tuna. Furthermore, a flat foil model that represents effectively only the posterior portion of a swimming fish leaves out any effects of the flows generated by the head, fins, and body thickness, which are known to greatly affect the hydrodynamic environment of the tail (Drucker and Lauder 2001, Standen and Lauder 2005, Tytell 2006).

5. Conclusion

While analyses of simple models are certainly successful in being able to isolate individual variables and their effects on swimming performance, our findings add to a growing body of work indicating that future studies will require more complex, 3D, and actively actuated biomimetic models in order to fully explore the mechanics and kinematics of fish swimming. Interactions between propulsive structures, driven by both muscular actuation morphology, and passive properties including stiffness, produce profoundly complex kinematics and hydrodynamic patterns. The difficulty in finding means of generalizing performance outcomes across different undulatory propulsors is no longer surprising. Engineers, biologists, and physicists must work together to develop more refined ways of investigating the interactions among motion and form to make progress in the study of the physics of fish swimming.

Acknowledgments

This work was supported by NSF Graduate Research Fellowship grants DGE-1144152 to KLF and KNL, National Science Foundation grant EFRI-0938043 and ONR MURI grant N00014-14-1-0533 (monitored by Dr Bob Brizzolara) to GVL, and NSF grant (IBN-9318065) to Prof Kathryn Dickson (Cal. State Fullerton) which supported the acquiring the data on tuna kinematics. Special thanks to Kathy Dickson for permission to use her tuna swimming kinematics data and for her helpful comments on the manuscript.

References

Affleck R J 1950 Some points in the function, development, and evolution of the tail in fishes *Proc. Zool. Soc. Lond.* **120** 349–68

Ahlborn B, Chapman S, Stafford R, Blake R W and Harper D G 1997 Experimental simulation of the thrust phases of fast-start swimming of fish *J. Exp. Biol.* **200** 2301–12

Akhtar I, Mittal R, Lauder G V and Drucker E 2007 Hydrodynamics of a biologically inspired tandem flapping foil configuration *Theor. Comput. Fluid Dyn.* **21** 155–70

Alexander R M 1965 The lift produced by the heterocercal tails of Selachii *J. Exp. Biol.* **43** 131–8

Anderson J M, Streitlien K, Barrett D S and Triantafyllou M S 1998 Oscillating foils of high propulsive efficiency *J. Fluid Mech.* **360** 41–72

Borazjani I and Daghooghi M 2013 The fish tail motion forms an attached leading edge vortex *Proc. R. Soc.* B **280** 20122071

Breder C M 1926 The locomotion of fishes *Zoologica* **4** 159–256

Chopra M G and Kambe T 1977 Hydromechanics of lunate-tail swimming propulsion. Part 2 *J. Fluid Mech.* **79** 49–69

Dewar H and Graham J 1994 Studies of tropical tuna swimming performance in a large water tunnel-energetics *J. Exp. Biol.* **192** 13–31

Dewey P A, Boschitsch B M, Moored K W, Stone H A and Smits A J 2013 Scaling laws for the thrust production of flexible pitching panels *J. Fluid Mech.* **732** 29–46

Donley J M and Dickson K A 2000 Swimming kinematics of juvenile kawakawa tuna (*Euthynnus affinis*) and chub mackerel (*Scomber japonicus*) *J. Exp. Biol.* **203** 3103–16

Drucker E G and Lauder G V 2001 Locomotor function of the dorsal fin in teleost fishes: experimental analysis of wake forces in sunfish *J. Exp. Biol.* **204** 2943–58

Ellerby D J, Altringham J D, Williams T and Block B A 2001 Slow muscle function of Pacific bonito (*Sarda chiliensis*) during steady swimming *J. Exp. Biol.* **203** 2001–13

Feilich K L and Lauder G V 2015 Passive mechanical models of fish caudal fins: effects of shape and stiffness on self-propulsion *Bioinspir. Biomim.* **10** 036002

Fierstine H L and Walters V 1968 Studies in locomotion and anatomy of scombroid fishes *Mem. Calif. Acad. Sci.* **6** 1–31

Gibb A C, Dickson K A and Lauder G V 1999 Tail kinematics of the chub mackerel *Scomber japonicus*: testing the homocercal tail model of fish propulsion *J. Exp. Biol.* **202** 2433–47

Kancharala A K and Philen M K 2014 Study of flexible fin and compliant joint stiffness on propulsive performance: theory and experiments *Bioinspir. Biomim.* **9** 036011

Karpouzian G, Spedding G and Cheng H K 1990 Lunate-tail swimming propulsion. Part 2. Performance analysis *J. Fluid Mech.* **210** 329–51

Katz J and Weihs D 1978 Hydrodynamic propulsion by large amplitude oscillation of an airfoil with chordwise flexibility *J. Fluid Mech.* **88** 485–97

Katz S L, Syme D A and Shadwick R E 2001 High-speed swimming: enhanced power in yellowfin tuna *Nature* **410** 770–1

Lauder G V, Flammang B and Alben S 2012 Passive robotic models of propulsion by the bodies and caudal fins of fish *Int. Comput. Biol.* **52** 576–87

Lighthill M J 1970 Aquatic animal propulsion of high hydromechanical efficiency *J. Fluid Mech.* **44** 265–301

Long J H 1992 Stiffness and damping forces in the intervertebral joints of blue marlin (*Makaira nigricans*) *J. Exp. Biol.* **162** 131–55

Long J H 1998 Muscles, elastic energy and the dynamics of body stiffness in swimming eels *Am. Zool.* **38** 771–92

Lucas K N, Thornycroft P J M, Gemmell B J, Colin S P, Costello J H and Lauder G V 2015 Effects of non-uniform stiffness on the swimming performance of a passively-flexing, fish-like foil model *Bioinspir. Biomim.* **10** 056019

McHenry M J, Pell C A and Long J H 1995 Mechanical control of swimming speed: stiffness and axial wave form in undulating fish models *J. Exp. Biol.* **198** 2293–305

Müller U K, Heuvel B, Stamhuis E and Videler J 1997 Fish foot prints: morphology and energetics of the wake behind a continuously swimming mullet (*Chelon labrosus* Risso) *J. Exp. Biol.* **200** 2893–906

Nauen J C and Lauder G V 2002 Hydrodynamics of caudal fin locomotion by chub mackerel, *Scomber japonicus* (Scombridae) *J. Exp. Biol.* **205** 1709–24

Quinn D B, Lauder G V and Smits A J 2014a Flexible propulsors in ground effect *Bioinspir. Biomim.* **9** 036008

Quinn D B, Lauder G V and Smits A J 2014b Scaling the propulsive performance of heaving flexible panels *J. Fluid Mech.* **738** 250–67

Quinn D B, Lauder G V and Smits A J 2015 Maximizing the efficiency of a flexible propulsor using experimental optimization *J. Fluid Mech.* **767** 430–48

Read D A, Hover F S and Triantafyllou M S 2003 Forces on oscillating foils for propulsion and maneuvering *J. Fluids Struct.* **17** 163–83

Root R G and Liew C W 2014 Computational and mathematical modeling of the effects of tailbeat frequency and flexural stiffness in swimming fish *Zoology* **117** 81–5

Sepulveda C and Dickson K A 2000 Maximum sustainable speeds and cost of swimming in juvenile kawakawa tuna (*Euthynnus affinis*) and chub mackerel (*Scomber japonicus*) *J. Exp. Biol.* **203** 3089–101

Shelton R M, Thornycroft P J M and Lauder G V 2014 Undulatory locomotion of flexible foils as biomimetic models for understanding fish propulsion *J. Exp. Biol.* **217** 2110–20

Standen E M and Lauder G V 2005 Dorsal and anal fin function in bluegill sunfish *Lepomis macrochirus*: three-dimensional kinematics during propulsion and maneuvering *J. Exp. Biol.* **208** 2753–63

Tytell E D 2006 Median fin function in bluegill sunfish *Lepomis macrochirus*: streamwise vortex structure during steady swimming *J. Exp. Biol.* **209** 1516–34

Westneat M W, Hoese W, Pell C A and Wainwright S A 1993 The horizontal septum: mechanisms of force transfer in locomotion of scombrid fishes (Scombridae, Perciformes) *J. Morphol.* **217** 183–204

Wolfgang M, Anderson J, Grosenbaugh M, Yue D and Triantafyllou M 1999 Near-body flow dynamics in swimming fish *J. Exp. Biol.* **202** 2303–27

Wu T Y 1971 Hydromechanics of swimming propulsion. Part 2. Some optimum shape problems *J. Fluid Mech.* **46** 521–44

Zhu Q 2007 Numerical simulation of a flapping foil with chordwise or spanwise flexibility *AIAA J.* **45** 2448–57